RSC Advances

ROYAL SOCIETY OF CHEMISTRY

www.rsc.org/advances

RSC Advances

ARTICLE

Ni-based catalyst derived from Ni/Al hydrotalcite-like compounds by urea hydrolysis method for CO methanation

Received 24th September 2015,
Accepted 00th January 20xx

DOI: 10.1039/x0xx00000x

www.rsc.org/

Li Bian[a,b], Weihan Wang[a], Rong Xia[a] and Zhenhua Li[a]*

The catalytic methanation of CO was investigated at atomospheric pressure over Ni-based catalyst derived from Ni/Al hydrotalcite-like compounds. The catalysts were prepared by the urea hydrolysis method and subjected to characterization in terms of XRD, TGA, N_2 adsorption-desorption, H_2-TPR, H_2-TPD and TEM. The H_2-TPD analysis reveals that an increase in Ni/Al molar ratio (0.5→2) served to increase Ni surface area (14.9→ 21.8 m^2/g) and nearly constant Ni surface area (22.3 m^2/g) was found at high Ni/Al molar ratios (>2), corresponding to a similar variation trend of CO conversion with Ni/Al molar ratio. The NA1 (Ni/Al molar ratio to 1) catalyst exhibited excellent stability at 600 °C for time on stream of 1800 min. The NA1 catalyst prepared from Ni/Al hydrotalcite-like compounds exhibits higher catalytic stability due to higher Ni dispersion and stronger resistance to coke deposition than the impregnated NA1-I catalyst.

1. Introduction

Natural gas, as a clean energy carrier, has attracted increasing attention worldwide due to less emissions of sulfur, nitrogen and dust than coal[1, 2]. In the last decade, production of synthetic natural gas (SNG) from coal was paid much attention, which provides a clean way for utilization of coal in regions rich of coal while lack of natural gas such as Korea and China[3-5]. This process includes coal gasification to syngas, water-gas shift reaction and methanation of syngas, in which methanation is the most critical step as shown in Equation (1) and (2)[6]. Even though CO methanation reaction has been widely applied for gas purification process in ammonia plant as well as removing traces of CO in H_2-rich gas in fuel cell industry[7-10], there are still many challenges for its application in coal to natural gas process.

$$3H_2 + CO \rightarrow CH_4 + H_2O \quad \Delta H = -206.28 kJ \cdot mol^{-1} \quad (1)$$

$$4H_2 + CO_2 \rightarrow CH_4 + 2H_2O \quad \Delta H = -164.94 kJ \cdot mol^{-1} \quad (2)$$

From thermodynamic point of view, carbon monoxide methanation is feasible [11, 12].However, methanation is a highly exothermic reaction and carbon deposition may result in deactivation of the catalyst. As reported, the catalyst used for methanation includes noble metals such as Ru and non-noble metals like Ni. It is well-known that Ru-based catalyst exhibits excellent catalytic activity and resistance to coke formation in the CO methanation. Unfortunately, it is expensive to limit its use in large-scale commercialization. Compared with Ru-based catalyst, Ni-based catalyst has nearly comparable activity with extra advantages like low cost and high methane selectivity[5, 13]. However, it is vulnerable to coke formation that makes the catalyst deactivated. Therefore, a prerequisite for commercial application of Ni catalyst in methanation of CO is to enhance its resistance capacity for coke formation.

Hydrotalcite-like compounds (HTlc), also known as layered double hydroxides (LDH) with the general formula $[M(II)_{1-x}M(III)_x(OH)_2]^{x+}[(A^{n-})_{x/n}\cdot yH_2O]^{x-}$, is a class of two-dimensional nanostructured anionic clays. The substitution of M^{2+} (M = Mg, Fe, Co, Cu, Ni, or Zn) by M^{3+} (M = Al, Cr, Ga, Mn or Fe) results in a net positive charge, attracting charge balancing anions to the interlayer region [14-18]. Complex oxides prepared from HTlc have been known to exhibit large metal surface area, high thermal stability and uniform distribution of active species [19-22]. As reported, the formation of small metallic nickel crystallites (6 nm) dispersed over NiO-alumina derived from HTlc can be achieved, which preserved the high activity of carbon dioxide methanation in 500 h lifetime tests even at high space velocity (268,800mL/g h) with only a little increase of Ni crystallite size (8.6 nm) and 11% coke deposit [23]. Feng et al.[24] pointed out that for the material prepared by calcination of NiAl-HTlc, NiO was reduced at higher temperature due to the stronger interaction between NiO and Al_2O_3 and higher nickel dispersion was achieved than that in the Ni/Al_2O_3 catalyst prepared by the impregnation method.

[a] Key Laboratory for Green Chemical Technology of Ministry of Education, Collaborative Innovation Center of Chemical Science and Engineering (Tianjin), School of Chemical Engineering & Technology, Tianjin University, Tianjin 300072, China. E-mail: zhenhua@tju.edu.cn;Tel.: +8622 87401818; Fax: +86 22 87401818
[b] College of Science, Hebei University of Engineering, Handan 056038, China.

However, Ni-Al_2O_3 catalyst derived from HTlc for carbon monoxide methanation has been few reported in open literatures. In this study, Ni-Al_2O_3 catalysts prepared from HTlc with a series of Ni/Al molar ratios were investigated for CO methanation. The samples were characterized by X-ray diffraction (XRD), thermogravimetric analysis (TGA), N_2 adsorption-desorption, transmission electron microscopy (TEM), H_2 temperature-programmed reduction (H_2-TPR) and H_2 temperature-programmed desorption (H_2-TPD). The catalytic activity and stability were tested to correlate the activity-structure relationship.

2. Experimental

2.1 Catalyst Preparation

The nickel aluminum composite oxides derived from HTlc in this study were prepared by the urea hydrolysis method (UHM). Certain amounts of $Ni(NO_3)_2 \cdot 6H_2O$ (98.0%, Tianjin Kermel Chemical Co., Ltd.), and $Al(NO_3)_3 \cdot 9H_2O$ (99.0%, Tianjin Kermel Chemical Co., Ltd.) with a specific molar ratios, as well as urea as the precipitant (99.0%, Tianjin Kermel Chemical Co., Ltd.) were dissolved in deionized water, being stirred for 30 min. Then the solution was transferred into an autoclave for hydrothermal treatment at 110 °C for 10 h. The solid obtained was separated by filtration, washed with deionized water until the filtrate solution became neutral (pH = 7), and dried at 110 °C for 24 h. Finally, the catalyst precursor was calcined at 650 °C for 6 h in air to obtain the nickel aluminum composite oxide. The Ni-Al composite oxide is labeled as NAx (x =0.5, 1, 2, 3 and 4) in which x represents the Ni/Al molar ratio. A reference Ni/Al_2O_3 catalyst with Ni/Al molar ratio as 1 was prepared by the conventional impregnation method (IPM), which was denoted as NA1-I. The Al_2O_3 support (Yixing Qianye non-metallic materials co., LTD) was pretreated at 500 °C for 4 h. Certain amounts of $Ni(NO_3)_2 \cdot 9H_2O$ was dissolved in the deionized water and followed by the addition of the Al_2O_3 support. The slurry was stirred at room temperature for 12 h and dried at 120 °C for 12 h in oven. The solid sample was calcined at 650 °C for 6 h in air.

2.2 Catalyst Characterization

XRD was conducted on a Rigaku C/max-2500 diffractometer using graphite filtered Cu Ka radiation (k=1.5406 Å) at 40 kV and 100 mA. The scanning rate was 5°/min and the scanning range was from 2θ=5°-90°. The average size of the Ni particle was calculated using the Scherrer equation. The TGA measurement of the sample was performed using STA449F3 (NETZSCH Corp.). The sample was heated under a flow in air (50 mL/min) from room temperature to 800 °C at 10°C /min. The reduction behavior of the oxides was studied by H_2-TPR using a Micromeritics AutoChem 2910 system equipped with a thermal conductivity detector (TCD). The catalyst (100mg) was loaded into a U-shape quartz tube and heated at 10 °C/min to 1000 °C in 10% H_2/Ar at a flow rate of 30 mL/min. H_2-TPD was performed using a Micromeritics AutoChem2910 system. The catalyst (100mg) was reduced at 650°C for 1 h under hydrogen flow (flow rate=30 mL/min) and then cooled to 100 °C under hydrogen flow. Then the flow of hydrogen was switched to argon at the same temperature and kept for 30 min to remove the weakly adsorbed hydrogen. Then the temperature was raised to 650 °C at a heating rate of 10 °C/min under Ar flow (flow rate=30 mL/min). The Ni metal surface area and dispersion were calculated by H_2-TPD.[25] N_2 adsorption-desorption were obtained at -196°C using a Micromeritics Tristar 3000 system. Before analysis, samples were outgassed at 300 °C for 4 h in a degas port of the analyzer. The surface area was calculated by the standard Brunauer-Emmet-Teller (BET) method, and the pore size distribution was determined from the Barrett-Joyner-Halenda (BJH) analysis based on the Kelvin equation[26]. Morphologies of the catalyst were characterized by TEM (Philips TECNAI G2F20). Samples for analysis were prepared by ultrasonic dispersion in ethanol and deposited on a micro-mesh copper grid.

2.3 Catalytic Activity Measurement

The methanation of CO was carried out at atmospheric pressure in a fixed bed quartz tube (i.d.=8 mm, length=550 mm) reactor. The catalyst bed was filled with 50 mg (40-60 mesh) catalyst diluted by 500 mg quartz sands (40-60 mesh). Prior to the reaction, the catalyst was reduced at 650 °C in situ for 1 h in pure H_2 stream (45 mL/min) and cooled down to the starting reaction temperature in N_2 (25mL/min). Then N_2/H_2/CO gas mixture with a fixed molar ratio of 1/6.75/2.25 (total flow rate = 250 mL/min) was fed through the catalyst bed at the GHSV of 300000 $mL \cdot g^{-1} \cdot h^{-1}$. The effluent product gases were cooled in a condenser followed by a dryer, and then analyzed by online gas chromatography using a TDX-01 packed column to quantitatively analyze N_2, CO, CH_4 and CO_2.

The CO methanation performance of the catalyst was evaluated in terms of CO conversion (X_{CO}), CH_4 selectivity (S_{CH4}), and CH_4 yield (Y_{CH4}) by the following formula.

$$X_{CO} = \frac{n_{CO(in)} - n_{CO(out)}}{n_{CO(in)}} \times 100\% \quad (3)$$

$$S_{CH_4} = \frac{n_{CH_4(out)}}{n_{CO(in)} - n_{CO(out)}} \times 100\% \quad (4)$$

$$Y_{CH_4} = X_{CO} \times S_{CH_4} \times 100\% = \frac{n_{CH_4(out)}}{n_{CO(in)}} \times 100\% \quad (5)$$

Where n_i is the molar flow rate of component *i* and subscripts *in* and *out* refer to the inlet and outlet gas stream.

3. Results and Discussion

3.1 Characterization of Catalyst Precursors

The XRD patterns (Fig.1) for all NAx precursors exhibit reflections at 2θ = 11.4°, 22.9°, 34.8°, 39.0°, 46.2°, and 61.3° that correspond to HTlc planes (003), (006), (009), (015), (018), and (110), respectively[27, 28]. The complete and sharp peaks

indicate well-crystallite HTlc structure. However, the weak signals at 2θ = 14.4°, 28.1°, and 48.9° belonging to the reflection of AlO(OH) (JCPDS NO.49-0133) were found only for NA0.5, suggesting that the other phase appeared on low Ni/Al molar ratio catalyst. The corresponding crystalline structural parameters (d spacing and lattice size) are listed in Table 1. The layer spacing d_{003}, d_{006} and d_{009} of catalyst precursors calculated based on the Braggs law, are similar with the values reported by Feng et al. [24].The lattice parameters a (=$2d_{110}$) and c (=d_{003} + $2d_{006}$ + $3d_{009}$) of the catalyst precursors are close to those of the pristine HTlc. The XRD analysis demonstrates that the NAx catalyst precursors have the typical HTlc structure.

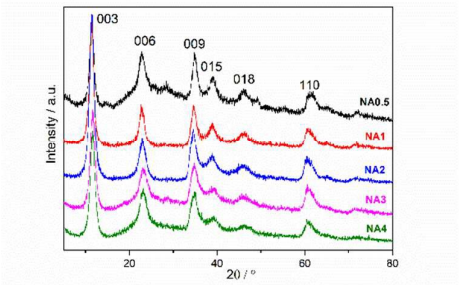

Fig.1 XRD patterns of the NAx precursors

Table 1 Analysis of XRD patterns for the NAx precursors

catalysts precursors	d_{003} (nm)	d_{006} (nm)	d_{009} (nm)	d_{110} (nm)	Lattice parameters	
					a(nm)	c(nm)
NiAl-HTlc[24]	0.76	0.38	0.24	0.15	0.30	2.28
NA0.5	0.78	0.39	0.26	0.15	0.30	2.35
NA1	0.78	0.39	0.26	0.15	0.30	2.34
NA2	0.78	0.39	0.26	0.15	0.30	2.34
NA3	0.78	0.39	0.26	0.15	0.30	2.34
NA4	0.77	0.39	0.26	0.15	0.30	2.33

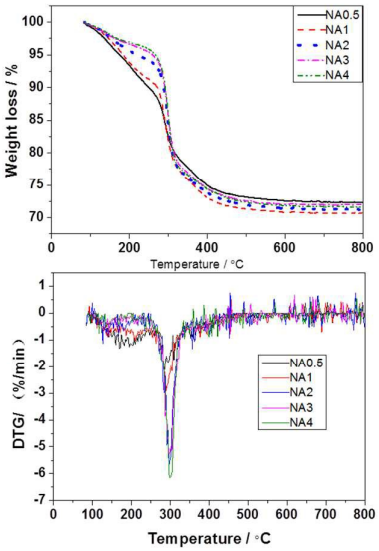

Fig.2 The TGA/DTG curves of the NAx precursors

The thermal decomposition of the NAx precursors has been evaluated by TGA/DTG and the results are presented in Fig. 2. The NAx precursors were decomposed in two stages at approximately 160-270 °C and 270-500°C, respectively[29, 30]. The former stage is corresponding principally to loss of hydration water, hydroxyls, carbon species such as CO_2, etc. The latter is corresponding to removal of species located in the interlaminar region. This decomposition of the interlayer is accompanied by the loss of hydroxyls in the form of H_2O and the loss of carbonate and nitrate anions in the form of CO_2 and NO_x[31]. The TGA/DTG curves became horizontal above 500 °C, showing that the precursors have been totally decomposed. This indicates that the layered structure of the precursors has been destroyed at temperature over 500 °C and composite NiAl oxides are obtained. In this paper, we chose 650°C as the calcination temperature during the catalyst preparation.

3.2 Characterization of Catalysts after Calcination

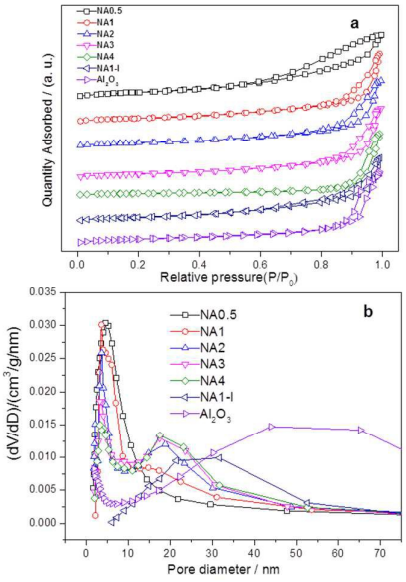

Fig.3 Textural properties of the catalysts after calcination (a) N_2 adsorption-desorption isotherm, (b) the pore size distribution

Table 2 The physisorption data of catalysts after calcination

Samples	BET surface area (m^2/g)	BJH pore volume (cm^3/g)	Average pore size (nm)
NA0.5	161.8	0.46	8.1
NA1	131.0	0.47	11.7
NA2	123.3	0.50	13.1
NA3	116.0	0.48	13.8
NA4	111.7	0.51	15.3
NA1-I	103.1	0.44	29.2
Al_2O_3	136.8	1.36	33.5

N_2 adsorption-desorption isotherms and pore size distribution profiles of the calcined samples are provided in Fig. 3. Fig. 3(a) shows that the hysteresis loops of NAx catalysts are typical characteristic of mesoporous material (Type IV). The hysteresis loops exhibit characteristics of both HI Type and H3 Type isotherms, demonstrating formation of both tubular and

parallel slit-shaped capillary pores due to the generated gas (CO_2, NO_x and vapor) diffusion in calcination process and the stacking of alumina microcrystallite[24]. Pore size distribution profiles in Fig. 3(b) show that NA0.5 and NA1-I catalysts are monomodal while NAx catalysts (x=1-4) are bimodal pore size distribution. The textural properties including specific surface area, pore volume and size of the Ni-based catalysts after calcination are summarized in Table 2. With Ni/Al molar ratio increase of NAx catalysts, the average pore size increased while the surface area decreased. The BET surface area, pore volume and average pore size of NA1-I were smaller than those of Al_2O_3. The NiO particles attached on the walls and/or in the mouth of the pores of Al_2O_3 may account for decrease of the BET area, inducing declining of pore volume and average pore size.

H_2-TPR curves for all the Ni-based catalysts are shown in Fig. 4. One broad hydrogen consumption peak was found for all the catalysts corresponding to reduction of nickel oxide to metallic nickel. The H_2-TPR measurements can be used to investigate the metal-support interaction and the reducibility of catalysts. Based on the metal-support interaction analysis, the reducible NiO species in the catalysts can be classified to several types: α-type, β-type and γ-type[32]. The low-temperature peak from 340 °C to 510 °C represents the reduction of α-type NiO species that has a weak interaction with the support [33, 34]. The middle peaks are assigned to the reduction of β-type NiO species that has a stronger interaction with support than α-type NiO species [35, 36]. The β-type NiO can be further classified into β_1-type (530~580 °C) and β_2-type (580~730 °C). The β_1-type NiO species with Ni-rich mixed oxide phase is more reducible than β_2-type NiO species with Al-rich mixed oxide phases[32, 34, 35]. The high-temperature peak (730~880 °C) is assigned to γ-type NiO species, which is attributed to the stable nickel aluminate with spinel structure [33-35]. The H_2 consumption peaks are fitted by Gaussian-type function in order to determine the proportion of different NiO species and the results are listed in Table 3. The impregnated NA1-I catalyst shows reduction peak in 340~640 °C belonging to a-type and β1-type without β_2-type and γ-type NiO species found, which had the weaker interaction between metal and support than NA1 catalyst derived from HTlc. The NA0.5 catalyst shows a broad peak (430~880 °C), which can be resolved to four peaks by Gaussian-type function: α-type, β_1-type, β_2-type and γ-type NiO (3.6%, 5.5%, 40.3% and 50.6% in Table 3, respectively), implying the relatively strong interaction of NiO with Al_2O_3, which could lead to the difficulty in reduction[37, 38] compared to NAx catalysts (x=1-4). The NAx (x=1-4) exhibit broad peaks in the range of 380~850 °C including α-type, β_1-type and β_2-type NiO species without γ-type NiO species in accordance with XRD results (Fig. 5). Cui et. al. found that moderate metal-support interaction is necessary to ensure the high activity and stability of the Ni/Al_2O_3 catalyst for syngas methanation at high temperatures[39]. NAx (x=1-4) catalysts had much more β-type reducible NiO species contrast to NA0.5and NA1-I, which should show the higher catalytic activity.

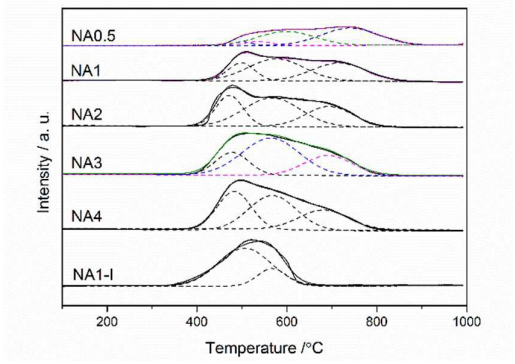

Fig.4 H_2-TPR profiles of the NAx catalysts and NA1-I catalyst after calcination

The reduction degree of the catalyst can be correlated to integrated area of the reduction peaks below 650 °C. To better understand reduction degree of the catalysts, the reducibility of NA4 calculated from the total integrated area of first two reduction peaks (below 650 °C) was defined as 100%. The relative reducibility of the catalyst was the ratio of the sum of its reduction peak areas below 650 °C and the sum of the reduction peak areas below 650 °C of NA4 catalyst. As listed in Table 3, the reduction degree of NAx catalyst increased with increase of Ni/Al molar ratio due to the weakened meta-support interaction. For Ni/Al molar ratio as 1, the reducibility of NA1-I was higher than that of NA1, on account of the bigger Ni particle size of NA1-I and weaker meta-support interaction[40].

Table 3 H_2-TPR quantitative data of the catalysts

Catalysts	Temperature (℃)				Integrated area				Fraction of total area (%)				Reducibility [a] (%)
	α	β_1	β_2	γ	A_α	$A_{\beta1}$	$A_{\beta2}$	A_γ	α	β_1	β_2	γ	
NA0.5	500	535	598	740	0.53	0.82	5.98	7.51	3.6	5.5	40.3	50.6	33.5
NA1	498	576	716	-----	3.41	7.12	8.87	-----	17.6	36.7	45.7	-----	48.1
NA2	471	566	694	-----	6.34	12.21	7.11	-----	24.7	47.6	27.7	-----	84.7
NA3	478	564	692	-----	5.56	15.69	7.27	-----	19.5	55	25.5	-----	97.1
NA4	482	567	682	-----	9.58	12.31	7.14	-----	33	42.4	24.6	-----	100.0
NA1-I	505	567	----	-----	14.83	3.8	-----	-----	79.6	20.4	-----	-----	85.1

[a]Calculated by:$(A_\alpha + A_{\beta1})/(A_\alpha + A_{\beta1})_{NA4} \times 100\%$, especially reducibility of NA0.5 calculated by:$(A_\alpha + A_{\beta1} + A_{\beta2})/(A_\alpha + A_{\beta1})_{NA4} \times 100\%$

Table 4 Physical and chemical properties of the catalysts

Samples	D[a] (%)	Nickel surface area ($m^2/(g_{\cdot Cat})$.)[a]	Particle size (nm)					activity per Ni surface area at 300℃ (mmol(CO)·($m^2/(g_{\cdot Cat})^{-1}$·min^{-1})
			d_{NiO}[b]	d_{Ni}[c]	d_{Ni}[d]	d_{Ni}[e]	d_{Ni}[f]	
NA0.5	5.9	14.9	8.2	13.8	—	—	—	3.79
NA1	5.4	18.6	8.7	14.8	19.5	15.4	20.4	6.66
NA2	4.7	21.8	9.0	15.2	—	15.8	—	6.47
NA3	4.4	22.3	9.2	15.3	—	16.6	—	6.17
NA4	4.0	22.4	9.5	16.1	—	—	—	6.27
NA1-I	3.6	12.7	21.4	22.5	27	29.2	34.1	2.29

[a]D, metal dispersion determined by H_2-TPD. [b]Determined by NiO(200) facet of the calcinated catalysts. [c] Determined by Ni(111) facet of the reduced catalysts. [d] Determined by Ni(111) facet of used catalysts at 600°C for 1800 min. [e] Mean size of Ni particle based on TEM analysis of the reduced catalysts. [f]Mean size of Ni particle based on TEM analysis of the used catalysts.at 600°C for 1800 min.

H_2-TPD was used to investigate the nickel dispersion and the nickel surface area for the Ni-based catalysts. As shown in Table 4, the dispersion of Ni species decreases in the order: NA0.5 > NA1> NA2 > NA3 > NA4. This may be attributed to the decreasing specific surface area with the increase of Ni/Al molar ratio in the NAx catalysts. So, the dispersion of Ni atom declines despite the higher Ni/Al molar ratio[41, 42].The nickel surface area which contributes active sites in the reaction is responsible for the catalytic performance. From Table 4, a significant increase of nickel surface area was found as the Ni/Al molar ratio increasing from 0.5 to 2, and then it stays nearly constant with further increasing the Ni/Al molar ratio from 2 to 4. It is noteworthy that both nickel dispersion and nickel surface area of NA1 catalyst derived from HTlc care much higher than those of the NA1-I catalyst.

The XRD patterns of the Ni-based catalysts after calcination are shown in Fig. 5. Diffraction peaks at 2θ = 37.4 °, 43.3 °, 63.3 °, 75.4 ° and 79.3 ° were detected for all the catalysts, corresponding respectively to NiO (111), (200), (220), (311) and (222) crystal planes [31]. The results demonstrated that HTlc structure completely collapsed after calcination at 650 °C and the NiO crystalline phases formed. The catalyst NA0.5 with a Ni/Al molar ratio of 0.5 could theoretically form stoichiometric $NiAl_2O_4$. Among NAx catalysts with different Ni/Al molar ratio, the peak corresponding to spinel phase $NiAl_2O_4$ was only observed for NA0.5 catalyst identifying with H_2-TPR results. While the other catalysts with Ni/Al molar ratio from 1 to 4 only showed diffraction peaks corresponding to NiO crystals without indicative peaks of Al_2O_3 or $NiAl_2O_4$ crystals. The catalysts with Ni/Al molar ratio (1→4) have excessive Ni to difficultly form stoichiometric $NiAl_2O_4$. Seo et. al [43] reported that the diffraction peaks of Al_2O_3 or $NiAl_2O_4$ were absent over the catalysts with the Ni/Al molar ratio (0.59→2.03) after calcination at 650 °C for 6h. However, the diffraction peak of $NiAl_2O_4$ appeared when the calcination temperature was raised to 800 °C and the associated crystallinity increased significantly with the increased calcinantion temperature, suggesting that the $NiAl_2O_4$ phase has a higher formation energy than NiO phase for Ni-Al_2O_3 catalysts derived from HTlc. Different from NA1 catalyst, the diffraction peaks at 32.9 °, 45.9 ° and 67.3 ° corresponding to Al_2O_3 were found on NA1-I. The NiO particle size on NA1-I is much bigger than that on NA1 catalyst as indicated by the sharp peak of NiO on NA1-I. All of these proved that the UMP method is more favorable for improving NiO dispersion on the catalyst than IPM method, which is in accordance with the characterization results of H_2-TPD.

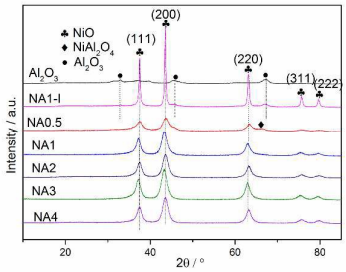

Fig.5 XRD patterns of the catalysts after calcination at 650 °C

3.3 Characterization of Reduced Catalysts

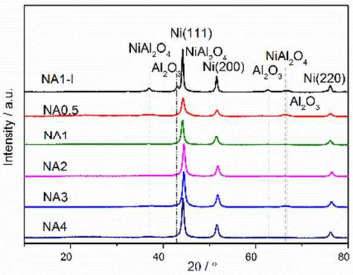

Fig.6 XRD patterns of the catalysts after reduction

Fig.6 shows the XRD patterns of the Ni-based catalysts after being reduced at 650°C for 1 h in H_2 stream. Diffraction peaks were detected at 44.2 °, 51.6 ° and 76.1 °, corresponding to Ni (111), Ni (200) and Ni (220) crystal planes. Ni particle sizes were calculated from Scherrer formula and the results were

listed in Table 4. Clearly, Ni particle size on NAx catalyst increased with increasing Ni/Al ratio. In addition, smaller Ni particle size was obtained on NA1 catalyst derived from HTlc than that on NA1-I (listed in Table 4).

The morphology of Ni particles is examined by TEM analysis and TEM images with particle size distribution histograms are presented in Fig.7. The reduced NAx catalysts display nearly spheric Ni particles and the average Ni particle sizes were 15.4, 15.8, and 16.6nm respectively for NAx (x=1-3) catalysts, while the Ni particle size of NA1-I was 29.2nm. TEM results further demonstrate that NAx from HTlc can get the Ni-based catalyst with smaller Ni particle size than the NA1-I impregnated catalyst.

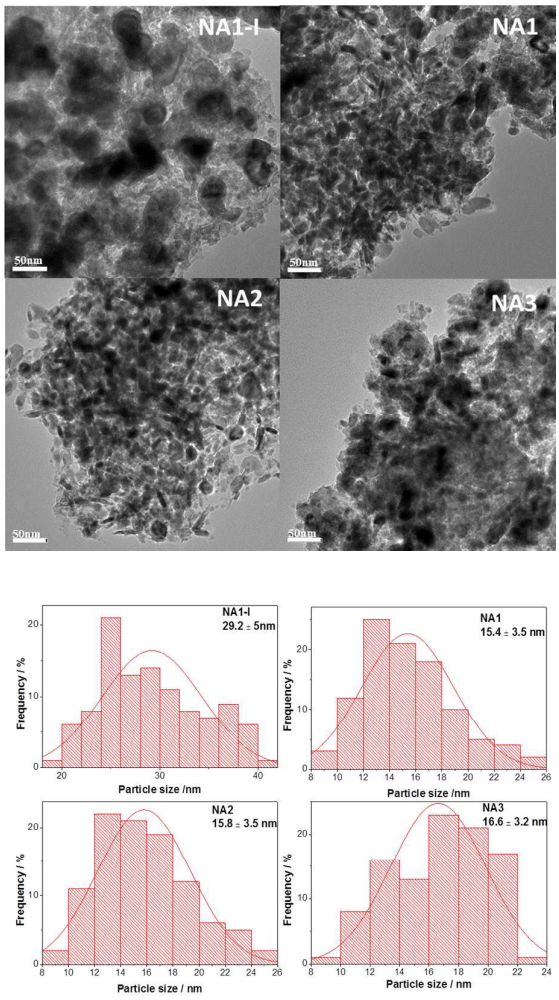

Fig.7 TEM images of the fresh catalysts after reduction

3.4 Catalyst Evaluation

3.4.1 Catalytic CO Methanation Activity on Different Catalysts

The catalytic activities of the Ni-based catalysts at 0.1 MPa and different temperatures (300°C −600 °C) are shown in Fig. 8. Fig.8(a) shows that a maximum CO conversion was observed at reaction temperature 400 °C-500 °C for NAx catalysts and nearly 100% CO conversion was achieved over NAx (x=1-4) catalysts. At lower temperature, CO conversion increased with temperature due to kinetics factors. However, at higher temperature CO conversion decreased due to the thermodynamic equilibrium limitation. Among NAx (x=0.5-4) catalysts, the NA0.5 with the lowest Ni/Al molar ratio exhibits the lowest activity. The CH_4 yield curves for all the catalysts are shown in Fig.8 (c). CH_4 yield first goes up and then declines as the reaction temperature increases. CO conversion as a function of Ni/Al molar ratio is shown in Fig. 8(d). It is clear that CO conversion increases with the Ni/Al molar ratio increase from 0.5 to 2, and then keeps nearly unchanged with further increasing the Ni/Al molar ratio from 2 to 4. From the fact that the variation trend of CO conversion with Ni/Al molar ratio is consistent with that of Ni surface area listed in Table 4, we can deduce that the Ni surface area is a key parameter affecting on the catalytic activity [43] in CO methanation. And bigger Ni surface area gives rise to higher catalytic activity. In

addition, NA1 catalyst displays better catalytic performance than NA1-I catalyst during reaction temperature range between 300°C to 600°C. This is also attributed to the bigger Ni surface area, the higher Ni dispersion and the smaller Ni particle size of NA1 catalyst than those of NA1-I catalyst as listed in Table 4. In addition, the activity per Ni surface area of the catalysts toward CO methanation at 300 °C are obtained, which follows the order of NA1> NA2 > NA4> NA3 >NA0.5> NA1-I. All these illustrated that NAx catalysts derived by HTlc have better methanation performance than the impregnated catalyst.

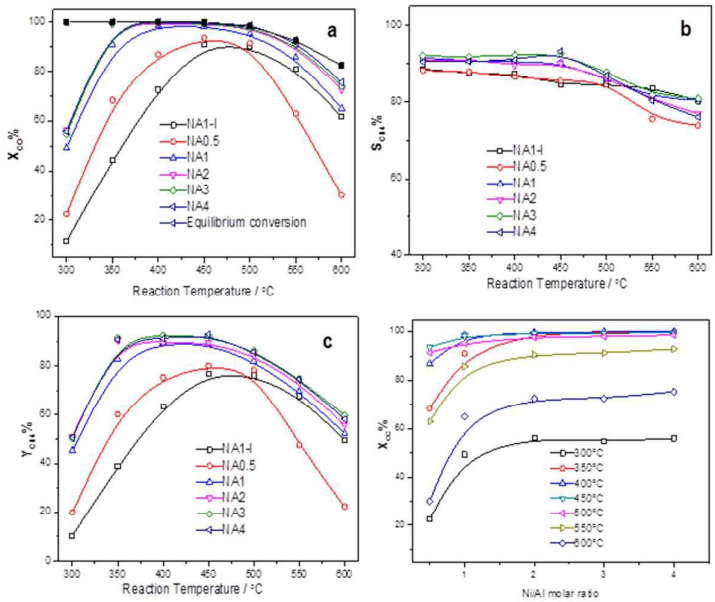

Fig.8 Catalytic performances of Ni catalysts at 0.1MPa and different reaction temperatures: (a) CO conversion, (b) CH_4 selectivity, (c) CH_4 yield; (d) CO conversion as a function of the Ni/Al molar ratio

3.4.2 Stability Test of CO Methanation

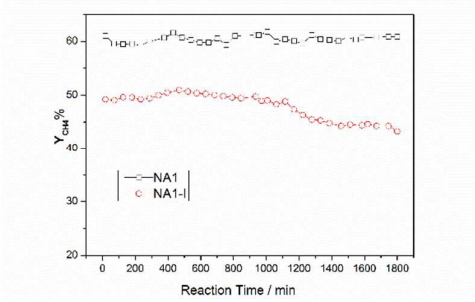

Fig.9 Stability result of CO methanation over NA1 and NA1-I catalysts at 600 °C and 0.1MPa.

The catalysts are expected to show not only high activity but also good stability. Especially, Ni-based catalyst usually undergoes carbon deposition and/or Ni aggregation at high reaction temperature, which may deteriorate the catalytic stability[44]. So, stability is a critical parameter for Ni-based catalyst on CO methanation performance. For these reasons, methane yields as a function of time over NA1 and NA1-I catalysts are tested (at 600 °C and 0.1MPa) and the results were shown in Fig.9. It is clear that the stability of NA1 catalyst is better than that of NA1-I catalyst. During the time period of 1800 min, methane yield was nearly kept unchanged on NA1 catalyst while methane yield decreased from 50% to 44% on NA1-I catalyst. These results demonstrated that catalyst of NA1 derived from HTlc exhibited greater high-temperature stability than the impregnated NA1-I catalyst.

3.5 Characterization of the Used Catalyst

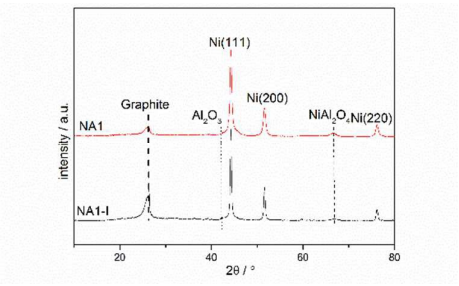

Fig.10 XRD patterns of the used catalysts

The catalysts after the above 1800 min stability test at 600 °C and 0.1MPa were subjected to characterization including XRD, TEM and TGA. The XRD patterns of the used catalysts are shown in Fig.10. Except for the signals corresponding to Ni (111), Ni (200) and Ni (220) as in the reduced catalyst, the diffraction peak at 2θ =26.4° is detected that is the characteristic of graphite, implying that carbon deposition

occurred during CO methanation process. The peak of graphite was more pronounced over the spent NA1-I catalyst than that over the spent NA1 catalyst, suggesting that the carbon deposition appeared more severe on the spent NA1-I catalyst. The intensities of Ni diffraction peaks of the used catalysts are higher and sharper than those reduced catalysts shown in Fig.6, demonstrating that Ni particles aggregation occurred to some extent during CO methanation process. As listed in Table 4, Ni particle size was increased from 14.8nm and 22.5 nm to 19.5 nm and 27 nm respectively on the used catalyst NA1 and NA1-I.

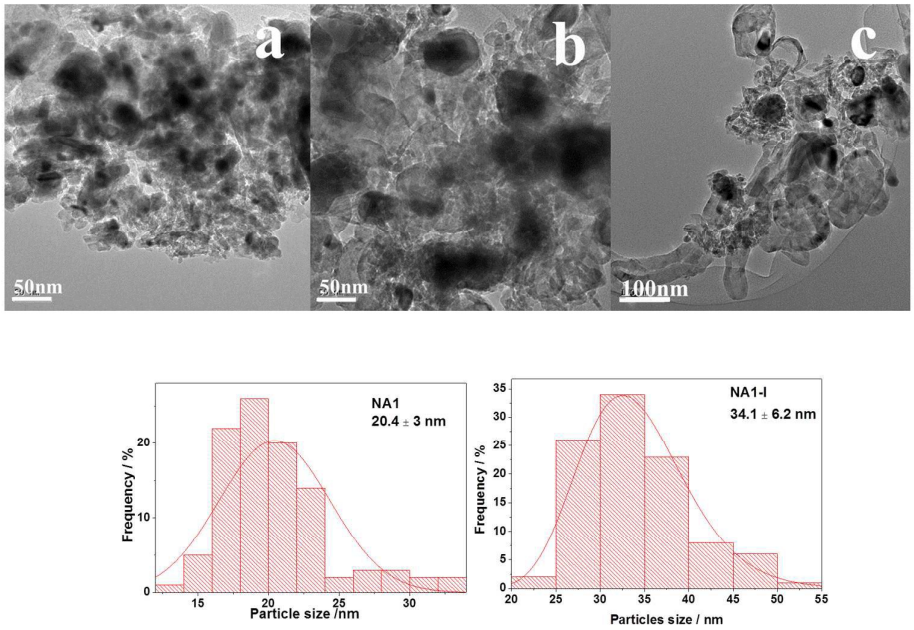

Fig.11 TEM images of the used catalysts: a: NA1, b and c: NA1-I

The morphology of the used catalysts is shown in Fig.11. Compared with the corresponding reduced NA1 and NA1-I catalysts as shown in Fig.7, the used catalysts (NA1 and NA1-I) exhibited increased Ni particle size, in accordance with the results of XRD. It is clear that the used NA1-I catalyst was encapsulated by deposited carbon. For NA1 catalyst, carbon deposition was not distinctly observed on the catalyst surface. Ni particles on the NA1 catalyst still remain mainly exposed. Therefore, the catalytic performance of NA1 at 600°C after 1800 min test did not decline. Combining the results of XRD and TEM, it could be seen that the deactivation of NA1-I was mainly owing to the deposition of large amounts of carbon species over the catalyst.

TG profiles of the reduced and used catalysts (a) and DTG profiles of the used catalysts (b) are shown in Fig.12. In Fig.12(a) the reduced catalysts gained a little weight over the temperature range 300 °C~500 °C owing to oxidation of the reduced Ni particles[45]. In Fig. 12, the used catalysts have two mass loss peaks due to coke combustion. It could be deduced that there are two kinds of carbon formed on the used catalysts, one is easily oxidized carbon species at temperature below 300 °C and the other is inactive carbon species being oxidized above 500 °C[46]. The carbon deposited on the catalyst could be originated from CO disproportionation and CH_4 decomposition[47]. The deposited carbon species corresponding to the weight loss below 300 °C is relatively active and can be oxidized, which is originated from CO disproportionation; the deposited carbon species corresponding to the weight loss above 500 °C is inert which cannot be removed until high temperature, deriving from CH_4 decomposition[44]. So, the carbon deposition of used catalysts mainly came from CH_4 decomposition. The carbon deposition amount (56.2%) on the used NA1-I catalyst is higher than that (27.5%) on the used NA1 catalyst. Therefore, the resistance of carbon deposition of NA1 is better than that of NA1-I. The weight loss temperature of NA1 (in Fig. 12 (b)) is 50 °C lower than that of NA1-I, indicating that carbon deposition on NA1 is more likely to be removed.

The Ni particle size was a key factor in carbon deposition. It was reported that bigger nickel particle is more favorable for coke formation[48-51]. Wang et al. found that coking formation took place mainly on large Ni particles and not on small ones during methane dry reforming[52]. Liu et al. have reported that the small-particle Ni catalyst was more active and stable than the large-particle Ni catalyst during CO methanation process[4]. The driving force for the carbon dissociation and diffusion would be smaller at the small Ni particle, and it was more difficult for the carbon to lift the Ni particle from the support because of stronger metal-support interaction[49, 53]. Compared with NA1 catalyst, NA1-I catalyst had bigger Ni particle size and

weaker interaction between Ni and Al_2O_3 support. Over the Ni particles of NA1-I, carbon deposition was easily dissociated from all directions and formed lots of graphite nucleated quickly which formed encapsulating carbon. So, no wonder that the coke deposition on the NA1-I catalyst is serious. Meanwhile, strong metal-support-interaction may also lead to more efficient electron transfer between metal and support to achieve a stable catalytic performance[54, 55]. Rossetti et al. reported that the strong interaction between metal and support could account for high glycerol conversion and a sufficient stability, whereas a weak interaction could lead to a decrease in the catalytic activity. NA1-I catalyst has bigger Ni size, weaker interaction between metal and support, and more severe carbon deposition than NA1 catalyst. Consequently, the NA1 catalyst can generate strong metal-support interaction with good Ni dispersion, showing strong resistance to coke formation, which contributes to its good stability.

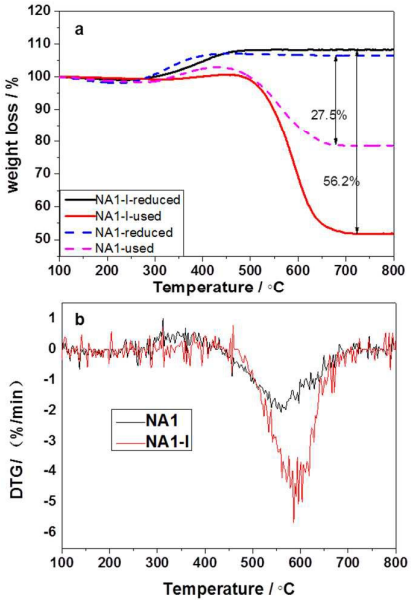

Fig. 12 TG profiles of the reduced and used catalysts (a) and DTG profiles of the used catalysts (b)

4 Conclusion

The Ni catalyst derived from HTlc precursors was developed for methanation of carbon monoxide. The characterization result of XRD demonstrated that the precursor of NAx catalyst is HTlc structure. N_2 adsorption-desorption and H_2-TPD results revealed that for NAx catalyst, both the specific surface area and Ni dispersion decrease with increasing Ni/Al molar ratio. But the Ni surface area increases first with Ni/Al ratio (0.5-2) and then keeps nearly unchanged at higher Ni/Al ratio than 2. Nearly 100% CO conversion of Ni-based catalysts with different Ni/Al molar ratio (1-4) was observed at reaction temperature between 400 °C and 500°C. The NA1 catalyst derived from HTlc exhibits better catalytic stability than the NA1-I catalyst, on account of the higher Ni dispersion, smaller Ni particle size and the stronger metal-support interaction leading to the stronger resistance to coke deposition.

References

1. Y. Zhang, G. Zhang, L. Wang, Y. Xu and Y. Sun, *Journal of Industrial and Engineering Chemistry*, 2012, **18**, 1590-1597.
2. S. Hwang, J. Lee, U. G. Hong, J. C. Jung, D. J. Koh, H. Lim, C. Byun and I. K. Song, *Journal of Industrial and Engineering Chemistry*, 2012, **18**, 243-248.
3. V. M. Lebarbier, R. A. Dagle, L. Kovarik, K. O. Albrecht, X. Li, L. Li, C. E. Taylor, X. Bao and Y. Wang, *Applied Catalysis B: Environmental*, 2014, **144**, 223-232.
4. Q. Liu, J. Gao, F. Gu, X. Lu, Y. Liu, H. Li, Z. Zhong, B. Liu, G. Xu and F. Su, *J. Catal.*, 2015, **326**, 127-138.
5. Q. Liu, J. Gao, M. Zhang, H. Li, F. Gu, G. Xu, Z. Zhong and F. Su, *RSC Advances*, 2014, **4**, 16094.
6. J. Kopyscinski, T. J. Schildhauer and S. M. A. Biollaz, *Fuel*, 2010, **89**, 1763-1783.
7. P. Panagiotopoulou, D. I. Kondarides and X. E. Verykios, *Applied Catalysis a-General*, 2008, **344**, 45-54.
8. F. B. Derekaya and G. Yaşar, *Catal. Commun.*, 2011, **13**, 73-77.
9. E. Kok, J. Scott, N. Cant and D. Trimm, *Catalysis Today*, 2011, **164**, 297-301.
10. H. Habazaki, M. Yamasaki, B. P. Zhang, A. Kawashima, S. Kohno, T. Takai and K. Hashimoto, *Applied Catalysis a-General*, 1998, **172**, 131-140.
11. R. B. Anderson, C. B. Lee and J. C. Machiels, *The Canadian Journal of Chemical Engineering*, 1976, **54**, 590-594.
12. R. B. Anderson, *The Journal of Physical Chemistry*, 1986, **90**, 4806-4810.
13. J. Gao, Q. Liu, F. Gu, B. Liu, Z. Zhong and F. Su, *RSC Advances*, 2015, **5**, 22759-22776.
14. K. Li, G. Wang, D. Li, Y. Lin and X. Duan, *Chinese Journal of Chemical Engineering*, 2013, **21**, 453-462.
15. F. R. Costa, M. Saphiannikova, U. Wagenknecht, G. Heinrich and B. Springer-Verlag, in *Wax Crystal Control: Nanocomposites, Stimuli-Responsive Polymers*, 2008, vol. 210, pp. 101-168.
16. F. Leroux and C. Taviot-Gueho, *Journal of Materials Chemistry*, 2005, **15**, 3628-3642.
17. C. Taviot-Gueho and F. Leroux, in *Layered Double Hydroxides*, eds. X. Duan and D. G. Evans, 2006, vol. 119, pp. 121-159.
18. F. Leroux and J. P. Besse, *Chemistry of Materials*, 2001, **13**, 3507-3515.
19. F. Zhang, X. Xiang, F. Li and X. Duan, *Catal. Surv. Asia*, 2008, **12**, 253-265.
20. K. Takehira and T. Shishido, *Catalysis Surveys from Asia*, 2007, **11**, 1-30.

21. F. Cavani, F. Trifirò and A. Vaccari, *Catal. Today*, 1991, **11**, 173-301.
22. S. Liu, D. Chen, K. Zhang, J. Li and N. Zhao, *Int. J. Hydrogen Energy*, 2008, **33**, 3736-3747.
23. S. Abelló, C. Berrueco and D. Montané, *Fuel*, 2013, **113**, 598-609.
24. J.-T. Feng, Y.-J. Lin, D. G. Evans, X. Duan and D.-Q. Li, *J. Catal.*, 2009, **266**, 351-358.
25. S. Velu and S. K. Gangwal, *Solid State Ionics*, 2006, **177**, 803-811.
26. E. P. Barrett, L. G. Joyner and P. P. Halenda, *Journal of the American Chemical Society*, 1951, **73**, 373-380.
27. D. G. Cantrell, L. J. Gillie, A. F. Lee and K. Wilson, *Applied Catalysis A: General*, 2005, **287**, 183-190.
28. M. Li, X. Wang, S. Li, S. Wang and X. Ma, *International Journal of Hydrogen Energy*, 2010, **35**, 6699-6708.
29. Z. P. Xu and H. C. Zeng, *Journal of Physical Chemistry B*, 2000, **104**, 10206-10214.
30. L. Chmielarz, P. Kuśtrowski, A. Rafalska-Łasocha and R. Dziembaj, *Thermochimica Acta*, 2002, **395**, 225-236.
31. L. Zhao, X. Li, Z. Qu, Q. Zhao, S. Liu and X. Hu, *Separation and Purification Technology*, 2011, **80**, 345-350.
32. J. Zhang, H. Xu, X. Jin, Q. Ge and W. Li, *Applied Catalysis A: General*, 2005, **290**, 87-96.
33. Y. Xu, H. Long, Q. Wei, X. Zhang, S. Shang, X. Dai and Y. Yin, *Catal. Today*, 2013, **211**, 114-119.
34. D. Hu, J. Gao, Y. Ping, L. Jia, P. Gunawan, Z. Zhong, G. Xu, F. Gu and F. Su, *Industrial & Engineering Chemistry Research*, 2012, **51**, 4875-4886.
35. A. Zhao, W. Ying, H. Zhang, H. Ma and D. Fang, *Catalysis Communications*, 2012, **17**, 34-38.
36. K. Y. Koo, H.-S. Roh, Y. T. Seo, D. J. Seo, W. L. Yoon and S. Bin Park, *International Journal of Hydrogen Energy*, 2008, **33**, 2036-2043.
37. J. Gao, C. Jia, J. Li, F. Gu, G. Xu, Z. Zhong and F. Su, *Ind. Eng. Chem. Res.*, 2012, **51**, 10345-10353.
38. J. Zhang, Z. Xin, X. Meng, Y. Lv and M. Tao, *Ind. Eng. Chem. Res.*, 2013, **52**, 14533-14544.
39. D. Cui, J. Liu, J. Yu, J. Yue, F. Su and G. Xu, *RSC Advances*, 2015, **5**, 10187-10196.
40. A. Y. Khodakov, A. Griboval-Constant, R. Bechara and F. Villain, *The Journal of Physical Chemistry B*, 2001, **105**, 9805-9811.
41. Y.-S. Jung, W.-L. Yoon, Y.-S. Seo and Y.-W. Rhee, *Catalysis Communications*, 2012, **26**, 103-111.
42. Y.-S. Jung, W.-L. Yoon, T.-W. Lee, Y.-W. Rhee and Y.-S. Seo, *Int. J. Hydrogen Energy*, 2010, **35**, 11237-11244.
43. Y.-S. Seo, Y.-S. Jung, W.-L. Yoon, I.-G. Jang and T.-W. Lee, *Int. J. Hydrogen Energy*, 2011, **36**, 94-102.
44. C. Guo, Y. Wu, H. Qin and J. Zhang, *Fuel Process. Technol.*, 2014, **124**, 61-69.
45. G. Wu, S. Li, C. Zhang, T. Wang and J. Gong, *Applied Catalysis B: Environmental*, 2014, **144**, 277-285.
46. D. Liu, X. Y. Quek, W. N. E. Cheo, R. Lau, A. Borgna and Y. Yang, *J. Catal.*, 2009, **266**, 380-390.
47. M. K. Nikoo and N. A. S. Amin, *Fuel Process. Technol.*, 2011, **92**, 678-691.
48. V. M. Gonzalez-DelaCruz, J. P. Holgado, R. Pereñíguez and A. Caballero, *J. Catal.*, 2008, **257**, 307-314.
49. D. Chen, K. O. Christensen, E. Ochoa-Fernández, Z. Yu, B. Tøtdal, N. Latorre, A. Monzón and A. Holmen, *J. Catal.*, 2005, **229**, 82-96.
50. K. O. Christensen, D. Chen, R. Lødeng and A. Holmen, *Applied Catalysis A: General*, 2006, **314**, 9-22.
51. A. J. Vizcaíno, A. Carrero and J. A. Calles, *Catal. Today*, 2009, **146**, 63-70.
52. N. Wang, W. Chu, T. Zhang and X. S. Zhao, *Int. J. Hydrogen Energy*, 2012, **37**, 19-30.
53. N. Wang, K. Shen, X. Yu, W. Qian and W. Chu, *Catalysis Science & Technology*, 2013, **3**, 2278.
54. V. Nichele, M. Signoretto, F. Menegazzo, A. Gallo, V. Dal Santo, G. Cruciani and G. Cerrato, *Applied Catalysis B: Environmental*, 2012, **111–112**, 225-232.
55. A. Iriondo, V. L. Barrio, J. F. Cambra, P. L. Arias, M. B. Guemez, M. C. Sanchez-Sanchez, R. M. Navarro and J. L. G. Fierro, *Int. J. Hydrogen Energy*, 2010, **35**, 11622-11633.